Lattice stability of some Ni-Ti alloy phases versus their chemical composition and disordering



2000 J. Phys.: Condens. Matter 12 L53

(http://iopscience.iop.org/0953-8984/12/5/101)

J. Phys.: Condens. Matter **12** (2000) L53–L60. Printed in the UK PII: S0953-8984(00)08186-8

**LETTER TO THE EDITOR**

# Lattice stability of some Ni–Ti alloy phases versus their chemical composition and disordering

W S Lai† and B X Liu

Department of Materials Science and Engineering, Tsinghua University, Beijing 100084, China
and
National Laboratory of Solid-State Microstructure, Nanjing University, Nanjing 210008, China

E-mail: wslai@tsinghua.edu.cn

Received 28 September 1999, in final form 23 November 1999

**Abstract.** A realistic *n*-body Ni–Ti potential is derived and applied in molecular dynamics simulation for studying the lattice stability of the terminal solid solutions and an intermetallic compound of B2 NiTi phase. It is found that when the solute contents are increased beyond two respective critical values of 15 at% of Ni and 38 at% of Ti, the crystalline lattices of the solid solutions become unstable and transform into amorphous states, suggesting that a glass-forming range of the system is from 15 to 62 at% of Ni. In the case of B2 NiTi compound, a crystalline-to-amorphous transition can result from the introduction of either a certain amount of chemical disordering or a compositional shift from its exact stoichiometry. In addition to the B2 NiTi phase, the simulation results also give some insight concerning the phase transition behaviour upon irradiation for the $Ni_3Ti$ and $NiTi_2$ intermetallic compounds.

It has been reported that some intermetallic compounds could undergo a crystalline-to-amorphous (C–A) transformation upon irradiation [1] and molecular dynamics (MD) studies have shown that the introduction of either chemical disordering or point defects into the crystalline lattices of the compounds could result in a C–A transition [2, 3]. Interestingly, in the Ni–Ti system, sharply different irradiation effects have been observed for three intermetallic compounds, i.e. the NiTi and $NiTi_2$ phases underwent amorphization, while the Ni-rich $Ni_3Ti$ phase transformed into a solid solution upon ion irradiation [4, 5]. As the damage introduced by ion irradiation in three intermetallic compounds in the Ni–Ti system is very similar, the difference in phase transition is mainly due to the variation of the chemical stoichiometry. Besides, it is well known that when a melt has a composition within the range of a stable solid solution, rapid solidification usually cannot quench the melt into a glass because the solid solution will always win the competition against glass and be formed readily [6]. Consequently, for a clear understanding of the irradiation-induced phase transition in the Ni–Ti intermetallic compounds as well as for determining the favoured composition for glass formation, it is necessary to study the lattice stability of the terminal solid solutions as a function of solute concentrations. Moreover, the NiTi phase is of simple CsCl (B2) structure, it is of interest to compare its phase stability upon irradiation with that of the $NiZr_2$ of complicated C16 structure, which has already been studied [2, 3]. We present the simulation results concerning the lattice stability of the terminal solid solutions as a function of solute contents and of the B2 NiTi while introducing chemical disordering or composition change.

† Corresponding author.

0953-8984/00/050053+08$30.00  

There is only one Ni–Ti potential derived by an embedded atom method reported in the literature by Farkas *et al* [7]. However, the application of the potential MD simulation is unable to reproduce the experimentally observed solid-state amorphization in the Ni–Ti multilayers and the potential cannot predict that the martensitic phase (B19′) is more stable than the B2 phase at low temperature either. The authors' view is that the physical properties used in deriving the potential were taken from the experimental cohesive energy of the B2 NiTi phase at high temperature [7] and the potential is therefore not relevant at least in some aspects. It is noted that the second-moment approximation of the tight-binding theory has been adopted to realistically derive some potentials for the fcc and hcp transition metals and alloys, yet not successfully for the bcc transition metals [8]. However, by including the higher-order (fourth), in addition to the second-order, moments of the electron density of states, the fourth-order moment approximation of the tight-binding theory can derive potentials with an appropriate precision for the bcc transition metals with partially-filled d-bands [9]. As the higher-order (fourth) moments of electron density of states describe the shape of the d-band, such potentials actually include angular force terms and thus can successfully reproduce the bulk properties and reconstruction of some surfaces of the bcc transition metals [9, 10]. It was noticed that the SMA and EAM were essentially the same and they included no angular force terms, yet they can successfully describe fcc transition metals with filled or nearly filled d-bands (especially Ni, Cu and metals within the same columns) with relative accuracy. Furthermore, it was found that the Ni–Zr potential derived from SMA by Massobrio *et al* [2] could be successfully applied to study the crystalline-to-amorphous transition of the intermetallic compound $NiZr_2$ upon ion irradiation [2] and our recent MD simulations based on the potential so derived were able to reproduce the solid-state amorphization in the Ni–Zr multilayers [11]. It is believed that the accuracy of the SMA potentials could be further improved for the fcc and hcp metals by including the fourth moment of the electron density of states, yet such inclusion requires approximately a factor of 100 more CPU time than standard EAM or SMA [10]. For simplicity, we adopt in the present study, SMA to construct a realistic Ni–Ti potential. Accordingly, the total energy of the system is given by

$$E = \sum_i \left\{ \sum_{j \neq i} A_{\alpha\beta} \exp\left[ -p_{\alpha\beta}\left(\frac{r_{ij}}{d_{\alpha\beta}} - 1\right)\right] - \sqrt{\sum_{j \neq i} \xi_{\alpha\beta}^2 \exp\left[ -2q_{\alpha\beta}\left(\frac{r_{ij}}{d_{\alpha\beta}} - 1\right)\right]} \right\} \qquad (1)$$

where $\alpha$ and $\beta$ indicate atomic species, $r_{ij}$ is the distance between the $i$ and $j$ atoms, and the indices $i$ ($j$) run over all the atoms. In the fitting procedure, we use the properties of the B2 phase at 0 K, instead of at high temperature, and they were taken from first principle calculation results, i.e. cohesive energy from the full-potential linear-muffin-tin-orbital (FLMTO) [12] and elastic constants from the full-potential linearized augmented-plane-wave (FLAPW) total-energy methods [13]. The parameters $A_{\alpha\beta}$, $p_{\alpha\beta}$, $\xi_{\alpha\beta}$ and $q_{\alpha\beta}$ are determined as follows: (i) for $\alpha = \beta$ a fit is performed on the cohesive energy, lattice parameters, elastic constants and the unrelaxed vacancy formation energy at 0 K of the pure elements Ni and Ti. The $d_{\alpha\alpha}$ is taken to be the nearest-neighbour distances of the pure elements Ni and Ti, respectively. (ii) For $\alpha \neq \beta$ the corresponding parameters are fitted on the cohesive energy and elastic constants of the B2 NiTi phase at 0 K [12, 13] and $d_{\alpha\beta}$ is taken to be the Ni–Ti nearest-neighbour distance in the B2 NiTi phase. The cutoff radius $r_c$ for atomistic interaction is also treated as an adjustable parameter for an optimized fitting and is determined to be 0.42 nm. Table 1 lists the obtained potential parameters after optimization and a comparison between the physical quantities reproduced by the potential and those used initially for fitting.

**Table 1.** Values of cohesive energy $E_c$, nearest-neighbour distances $d$, elastic constants $C_{ij}$, and vacancy formation energy $E_v^f$, which are used for the fit of the potential (see text), and potential parameters $A_{\alpha\beta}$, $p_{\alpha\beta}$, $\xi_{\alpha\beta}$ and $q_{\alpha\beta}$ for Ni–Ni, Ti–Ti and Ni–Ti. $E_c$, $A_{\alpha\beta}$, and $\xi_{\alpha\beta}$ are expressed in eV/atom, $d$ in Å, $C_{ij}$ in eV Å$^{-3}$, and $E_v^f$ in eV.

| | Ni | | Ti | | Ni–Ti | |
|---|---|---|---|---|---|---|
| | This work | Experimental | This work | Experimental | This work | FLMTO or FLAPW |
| $E_c$ | 4.44 | 4.44[a] | 4.85 | 4.85[a] | 5.02 | 5.02[b] |
| $d$ | 2.49[a] | | 2.95[a] | | 2.607[c] | |
| $C_{11}$ | 1.568 | 1.629[d] | 1.103 | 1.0992[d] | 1.279 | 1.112[e] |
| $C_{12}$ | 1.085 | 0.943[d] | 0.549 | 0.5452[d] | 0.846 | 0.921[e] |
| $C_{13}$ | | | 0.465 | 0.4263[d] | | |
| $C_{33}$ | | | 1.187 | 1.1891[d] | | |
| $C_{44}$ | 0.729 | 0.824[d] | 0.193 | 0.3171[d] | 0.297 | 0.306[e] |
| $E_v^f$ | 1.65 | 1.60[f] | 1.56 | 1.55[g] | | |
| $A$ | 0.104 | | 0.153 | | 0.3 | |
| $p$ | 11.198 | | 9.253 | | 7.9 | |
| $\xi$ | 1.591 | | 1.879 | | 2.48 | |
| $q$ | 2.413 | | 2.513 | | 3.002 | |

[a] [14]. [b] [12]. [c] [15]. [d] [16]. [e] [13]. [f] [17]. [g] [18].

In addition, the cohesive energies and the lattice constants of some other Ni–Ti metastable and equilibrium crystalline phases are also reproduced by the constructed potential and are listed in table 2 together with a comparison between the reproduced ones with those from first principle calculations [12] or experimental studies [15, 19]. Obviously, for the NiTi phase at 0 K, the potential predicts that the martensitic phase (B19′) possesses the largest cohesive energy, which is 0.018 and 0.118 eV/atom greater than those of B2 and $L1_0$, respectively. One sees that the potential is also able to reproduce the cohesive energy and lattice constants at 0 K for the $D0_{24}$ $Ni_3Ti$ phase, even though these experimental values were not used in the fitting procedure. Besides, the cohesive energy of the $D0_{24}$ $Ni_3Ti$ phase is derived by the potential to be 0.01 eV larger than that of $L1_2$ $Ni_3Ti$, revealing an energetic sequence of these two phases that is compatible with reality. To further verify the potential, some other thermodynamic properties, e.g. enthalpy and volume, of the B2 NiTi phase are also calculated based on MD simulations in a B2 NiTi model consisting of $10 \times 10 \times 10$ unit cells ($= 2000$ atoms) with periodic boundary conditions. The MD simulations are carried out with Parrinello–Rahman molecular-dynamics scheme [20] and the equations of motion are integrated using a fourth-order predictor-corrector algorithm of Gear with a time step $t = 5 \times 10^{-15}$ s. Figure 1 shows the variation of the enthalpy ($H$) and volume ($V$) of B2 NiTi versus temperature. One observes that an abrupt change for $H$ and $V$ appears under the same temperature regime. A melting point of the B2 NiTi phase is thus estimated to be of 1612–1653 K. In addition, melting at $T = 1653$ K is confirmed by a set of calculated liquid-like curves of the pair-correlation functions. Consequently, the computed melting point is in excellent agreement with the experimental one of 1583 K, as an overheating of a perfect crystal model is unavoidable and an overestimated value of $\approx$70 K is reasonable. Based on the above discussion, the derived Ni–Ti potential can be considered a realistic one, as it can reproduce those static and dynamic properties of some alloy phases in the Ni–Ti system.

The simulation models consist of $8 \times 8 \times 8 \times 4 = 2048$ atoms for fcc Ni crystalline and $10 \times 6 \times 6 \times 4 = 1440$ atoms for hcp Ti crystalline lattices, respectively. In both models, the [100] and [001] crystalline directions are parallel to the $x$- and $z$-axes, respectively, and the crystalline directions along the $y$-axis are [010] for fcc Ni and [120] for hcp Ti, respectively.

**Table 2.** A comparison of the physical properties derived from the constructed potential with those from FLMTO calculations and experiments for some Ni–Ti metastable and equilibrium crystalline alloy phases. The cohesive energy $E_c$ is expressed in eV/atom, lattice constants $a$, $b$, $c$ in Å.

| Phase | Property | Experimental | FLMTO[a] | This work |
|---|---|---|---|---|
| B19′ NiTi | $E_c$ | | 5.04 | 5.038 |
| | $a$ | | | 2.956 |
| | $b$ | | | 4.455 |
| | $c$ | | | 4.189 |
| | $\gamma$ | | | 93.26 |
| B2 NiTi | $E_c$ | 4.95[b] | 5.02 | 5.02 |
| | $a$ | 3.01[b] | | 3.01 |
| $L1_0$ NiTi | $E_c$ | | 4.97 | 4.92 |
| | $a$ | | | 3.784 |
| $D0_{24}$ $Ni_3Ti$ | $E_c$ | 4.86[b], 4.987[c] | 5.036 | 4.936 |
| | $a$ | 5.10[b] | | 5.15 |
| | $c$ | 8.30[b] | | 8.35 |
| $L1_2$ $Ni_3Ti$ | $E_c$ | | 5.031 | 4.926 |
| | $a$ | | | 3.633 |

[a] [12]. [b] [15]. [c] [19].

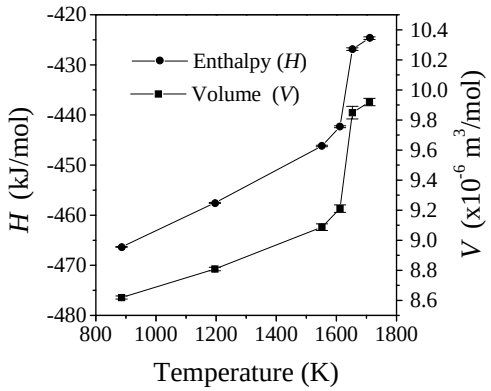


**Figure 1.** Variation of the enthalpy $H$ and the volume $V$ in the model of B2 NiTi crystal as functions of temperature.

The periodic boundary conditions are adopted in all three directions. The solute atoms are added by the random substitution of a certain number of Ti (Ni) atoms into the Ni fcc (Ti hcp) lattice. To avoid forming a cluster of solute atoms, the random substitution is performed in each unit cell of Ni fcc (Ti hcp) lattice with the same probability, and the initial fcc Ni-rich (hcp Ti-rich) solid solution is thus obtained. Molecular dynamics simulation is performed for the solid solutions with gradually increasing the solute concentration to find out the critical compositions, at which crystalline lattices of the solid solutions become unstable and transform into a disordered state. After construction of the models, simulation is then run at 300 K for 20 000 MD time steps to a relatively equilibrium state, at which all the related dynamic variables show no secular variation. The temperature of the simulated system is maintained by a time-to-time rescaling of the velocities of atoms to the assigned temperature at every 100 time steps, if an average deviation from the assigned one is over 1 K. The process of structural change in the above Ni–Ti models is monitored by the pair-correlation function $g(r)$, which is commonly recognized as a decisive parameter with which to identify an amorphous structure.

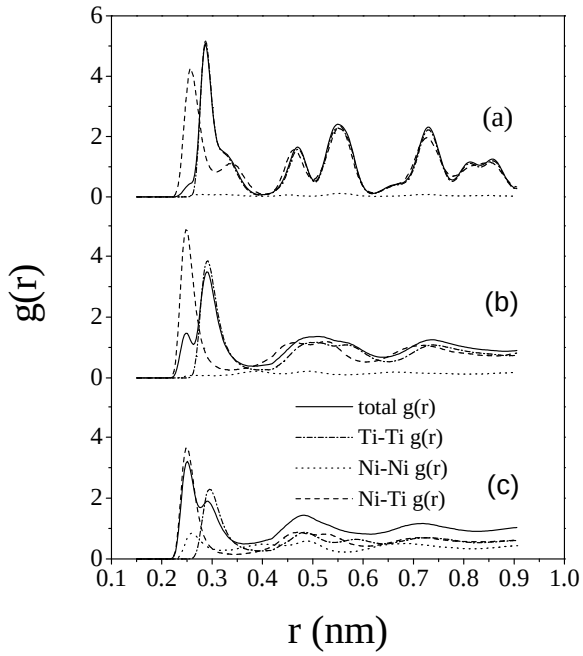


**Figure 2.** Total and partial pair-correlation functions for the hcp Ti-rich solid solution from simulations performed at 300 K for 20 000 MD time steps. The compositions are at: (a) 5 at%, (b) 15 at% and (c) 40 at% of Ni, respectively. The full curve is for the total $g(r)$; the dotted curve is for Ni–Ni $g(r)$; the short dashed curve is for Ni–Ti $g(r)$; and the dot-dashed line is for Ti–Ti $g(r)$.

Figure 2 displays the total and partial pair-correlation functions $g(r)$ calculated for the Ti-rich hcp solid solutions consisting of Ni solute atoms up to 5, 15 and 40 at%, respectively. From the figure, one sees that the solid solutions with 5 at% of Ni still retain the hcp crystalline structure. While for the solid solution with 15 or 40 at% of Ni, a C–A transition apparently takes place, as evidenced by the shape of the $g(r)$ curves commonly observed for the amorphous alloys. A similar simulation is also performed for the Ni-rich fcc solid solutions with various compositions and the C–A transition is observed when the Ti solute contents are greater than 38 at%.

To obtain firm evidence for a C–A transition, the molar enthalpy and volume were calculated as a function of alloy composition and are displayed in figure 3. One sees that from the Ti end, the enthalpy and volume both decrease with increasing of Ni content and that at $x_{Ni} = 15$ at% the slopes of enthalpy and volume are discontinuous with a clear kink in volume, confirming a C–A transition, which is the same as determined by the pair correlation function calculation already mentioned. While at the Ni side, there is a sudden drop in molar enthalpy at $x_{Ti} = 38$ at%. In addition, the volume variation of the fcc Ni solid solutions with increasing of Ti content increases gradually and a kink appears at $x_{Ti} = 38$ at%, confirming a C–A transition at this composition. The volume expansion of the Ni solid solution with increasing Ti content is caused by soluting Ti with a larger atomic radius into the fcc lattice and a sudden volume increase at $x_{Ti} = 38$ at% is associated with the formation of a Ni-rich Ni–Ti amorphous phase, which possesses a couple of per cent extra free volume than that of its crystalline counterpart [21]. According to the above results, the required compositions for C–A transition to take place are deduced to be 15 at% of Ni and 38 at% of Ti for hcp Ti-rich and the fcc Ni-rich solid solutions, respectively. It is found that in a central composition region between 15–62 at% of

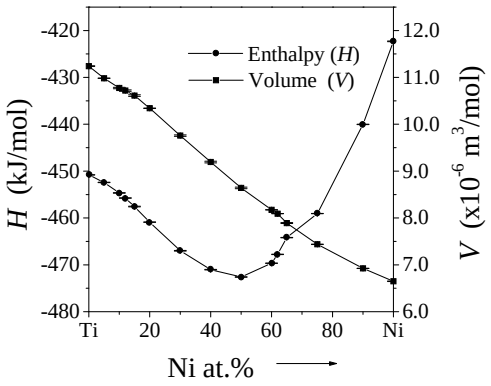


**Figure 3.** The molar enthalpy and volume of the system at a relative equilibrium state versus compositions obtained from simulations performed at 300 K for 20 000 MD time steps from the Ni-rich fcc solid solution (0–50% Ti) and Ti-rich hcp solid solution (50–100% Ti).

Ni, the supersaturated solid solutions are unstable and will turn into an amorphous state. In other words, this composition range is favoured for spontaneous vitrification and can therefore be considered as the glass-forming range of the Ni–Ti system. It should be noted that the above calculated solubilities of supersaturated solid solutions are the non-equilibrium ones, which can be obtained in the experiments only by non-equilibrium processes, such as mechanical alloying, ion mixing (IM), etc. To verify the calculated solubilities of the supersaturated solid solutions, we specially designed the Ni–Ti multilayered samples with various overall compositions and performed IM experiments. The IM results turn out to be in good agreement with those obtained from simulations within an experimental error of 5%. For instance, IM experiments determined the maximum supersaturated solid solubility of Ti in Ni to be less than 37 at%, as it was observed that Ni-based solid solutions are obtained by IM within a composition range from 0 to 37 at% of Ti, while a unique amorphous phase is formed with the alloy composition being beyond the maximum solubility.

To study the possible amorphization of B2 NiTi upon ion irradiation, another model was constructed and it consisted of $10 \times 10 \times 10$ unit cells ($= 2000$ atoms) of B2 NiTi crystal with periodic boundary conditions. In our case, the chemical disordering was introduced by anti-site defects through random exchanging of the Ni and Ti atoms and this method is similar to that reported by Massobrio *et al* [2]. For quantitative characterization of the disordering, a long-range order (LRO) parameter was adopted. The LRO parameter was defined as $\eta = (p - \gamma)/(1 - \gamma)$, where $p$ and $\gamma$ are the probabilities of the presence of an $A$-type atom (A = Ni or Ti) on its own lattice site and the molar ratio of $A$ atoms in B2 crystal, respectively. The lattice stability of B2 NiTi phase with increasing chemical disordering, i.e. decreasing $\eta$, was studied at room temperature ($= 300$ K) to determine the critical value of $\eta$ for C–A transition to take place.

Figure 4 gives the variations of molar enthalpy and of volume as a function of the LRO parameter $\eta$ in B2 NiTi crystal at its exact stoichiometry after simulations performed at 300 K for 20 000 MD steps. One sees that with decreasing $\eta$ both enthalpy and volume increase gradually and remain unchanged after reaching a plateau at about $\eta \leqslant 0.4$, at which a C–A transition takes place. The C–A transition taking place at $\eta \leqslant 0.4$ was also confirmed by the corresponding pair-correlation functions calculation, as the resultant curves are similar to those given in figure 2(c). An estimation of the volume expansion after C–A transition was found to be 4%, which is compatible with the theoretical model for the amorphous structure

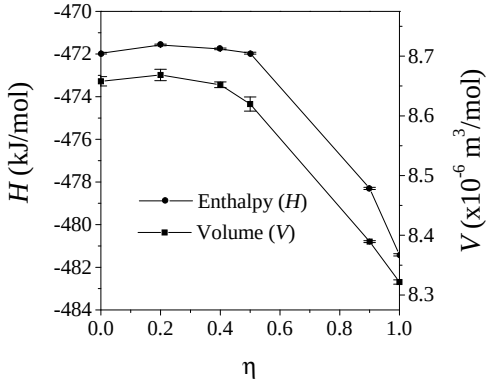


**Figure 4.** Variation of the molar enthalpy $H$ and the volume $V$ as a function of the LRO parameter $\eta$ in the model of B2 NiTi crystal obtained by averaging data between 20 000 and 21 000 MD steps.

[21]. It has been reported that in the $NiZr_2$ phase of the complicated C16 structure, a C–A transition took place at $\eta \leqslant 0.6$ [2]. Our results seem to suggest that the B2 NiTi phase is more stiff than the $NiZr_2$ phase in terms of irradiation stability, as the NiTi phase needs much more chemical disordering ($\eta \leqslant 0.4$) to transit into an amorphous state.

We also studied the lattice stability of the B2 NiTi phase as a function of composition variation by random substitution of Ni with Ti atoms or *vice versa* in B2 crystal at the eutectic temperature (1391 K), which corresponds to the broadest composition range for the B2 phase in the equilibrium phase diagram. It turns out that when the Ni concentration is in the range of 49.5–57.0 at% the crystalline lattice of B2 phase is stable, yet outside this composition range the lattice becomes unstable and melting takes place within our simulation time (20 000 MD steps). These results are in good agreement with those shown in the equilibrium phase diagram, i.e. the composition range of the B2 phase is between 49.5 and 57.0 at% Ni.

It is interesting to note that the structural transition behaviours of three Ni–Ti intermetallic compounds, i.e. $NiTi_2$, NiTi and $Ni_3Ti$, upon ion irradiation to an adequate dose are different, i.e. the NiTi and $NiTi_2$ phases underwent amorphization while the $Ni_3Ti$ phase transformed into a solid solution [4, 5]. These experimental observations can be well understood based on our simulation results. It is known that the ion irradiation process can generally be divided into two steps, i.e. a first step of atomic collision cascade and a second step of relaxation [22]. In the first step, the irradiating ions induce a series of atomic collisions, namely atomic collision cascades, which drive the crystalline structure of the above three Ni–Ti intermetallic compounds into a highly disordered state with an elevated energy. In the following step of relaxation lasting only for $10^{-10}$–$10^{-9}$ s, the disordered structure can only transform into simple structured crystalline phase or still stay in a disordered atomic configuration. According to our simulation results, the compositions of $NiTi_2$ and NiTi phases fall in the glass-forming range, i.e. in this range the solid solution is unstable in comparison with an amorphous state. As a result, they can only stay in a disordered state rather than crystallize into a simple structured solid solution. While for the $Ni_3Ti$ phase, since its structure is very complicated, it cannot crystallize in its own structure during relaxation. Furthermore, its composition falls off outside the glass-forming range, meaning the solid solution is more favoured than an amorphous state. That is why the $Ni_3Ti$ transformed into a solid solution upon ion irradiation. In short, the different behaviour in irradiation-induced phase transitions of $NiTi_2$, NiTi and $Ni_3Ti$ are attributed to their alloy compositions, which are either favoured or not for the glass formation.

In conclusion, we have derived an $n$-body Ni–Ti potential, which is capable of reproducing some static and dynamic properties of some Ni–Ti alloy phases. Employing the potential, the glass-forming ability of the system is determined by molecular dynamics simulation of the Ni- and Ti-rich solid solutions and is in good agreement with the experimental observations. Besides, simulation can also give a relevant explanation to the observed phase transition behaviours of three Ni–Ti intermetallic compounds upon ion irradiation.

This study is supported by the National Natural Science Foundation of China. Partial financial aid from the Tsinghua Administration is also gratefully acknowledged.

## References

[1] Russell K C 1985 *Prog. Mater. Sci.* **28** 229
[2] Massobrio C, Pontikis V and Martin G 1990 *Phys. Rev.* B **41** 10 486
[3] Devanathan R, Lam N Q, Okamoto P R and Meshii M 1993 *Phys. Rev.* B **48** 42
[4] De Tendler R H, Rodriguez C, Gallego L J and Alonso J A 1996 *J. Mater. Sci.* **31** 6395
[5] Moine P and Jaouen C 1993 *J. Alloys Compounds* **194** 373
[6] Egami T 1996 *J. Non-Cryst. Solids* **205–207** 575
[7] Farkas D, Roqueta D, Villette A and Ternes K 1996 *Modelling Simulation Mater. Sci. Eng.* **4** 359
[8] Cleri F and Rosato V 1993 *Phys. Rev.* B **48** 22
[9] Carlsson A E 1991 *Phys. Rev.* B **44** 6590
[10] Xu W and Adams J B 1994 *Surf. Sci.* **301** 371
[11] Lai W S and Liu B X 1998 *Phys. Rev.* B **58** 6063
[12] Pasturel A, Colinet C, Nguyen Manh D, Paxton A T and van Schilfgaarde M 1995 *Phys. Rev.* B **52** 15 176
[13] Bihlmayer G, Eibler R and Neckel A 1994 *Phys. Rev.* B **50** 13 113
[14] Kittel C 1986 *Introduction to Solid State Physics* (New York: Wiley)
[15] Hultgren R, Desai P D, Hawkins D T, Gleiser M and Kelly K K 1973 *Selected Values of Thermodynamic Properties of Binary Alloys* (Metals Park, OH: ASM)
[16] Simmons G and Wang H 1971 *Single Crystal Elastic Constants and Calculated Aggregate Properties: A Handbook* (Cambridge, MA: MIT)
[17] Wycisk W and Feller-Knipmeier M 1978 *J. Nucl. Mater.* **69/70** 616
[18] Shestopal V O 1966 *Fiz. Tverd. Tela (Leningrad)* **7** 3461 (Engl. Transl. *Sov. Phys. Solid State* **7** 2798)
[19] Esin Yu O, Valishev M G, Ermakov A F, Gel'd O v and Petrushevsku M S 1981 *Russ. J. Phys. Chem.* **55** 421
[20] Parrinello M and Rahman A 1981 *J. Appl. Phys.* **52** 7182
[21] van den Beukel A and Radelaar S 1983 *Acta Metall.* **31** 419
[22] Liu B X and Jin O 1997 *Phys. Status Solidi* A **161** 3